
Supplementary materials

Kinetic modelling of the aqueous-phase reforming of Fischer-Tropsch water over ceria-zirconia supported nickel-copper catalyst

Irene Coronado[a,1], Aitor Arandia[b,1,*], Matti Reinikainen[a], Reetta Karinen[b], Riikka L. Puurunen[b] and Juha Lehtonen[a]

[a] VTT Technical Research Centre of Finland Ltd., Espoo, FI-02044 VTT, Finland
[b] Aalto University, Department of Chemical and Metallurgical Engineering, P.O. Box 16100, FI-00076 Aalto, Finland
[1]Both authors contributed equally to this work.
*Corresponding author: *aitor.arandiagutierrez@aalto.fi*

Appendix A. Individual conversions of oxygenated hydrocarbons in the APR of FT water

The individual conversions for each oxygenated compound present in the feed and calculated by using Eq. 33, are presented in Figure S1 and Figure S2 for 3.2 and 4.5 MPa, respectively. Negative conversions observed for some of the compounds intend to quantify the production of additional amounts of those compounds that were originally present in the feedstock.

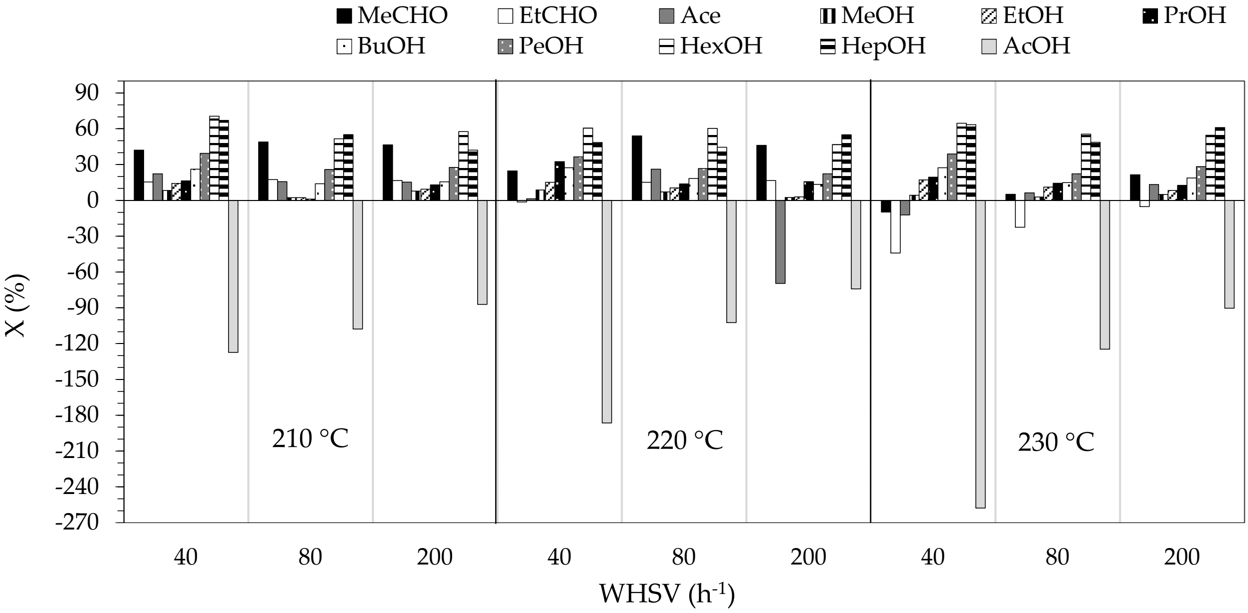

Figure S1. Individual conversion of ethanal (black), propanal (white), acetone (dark grey), methanol (vertical lines), ethanol (diagonal lines), propanol (black with white dots), butanol (white with black dots), pentanol (grey with white dots), hexanol (thin horizontal lines), heptanol (thick horizontal lines), and acetic acid (light grey) in APR at 3.2 MPa.

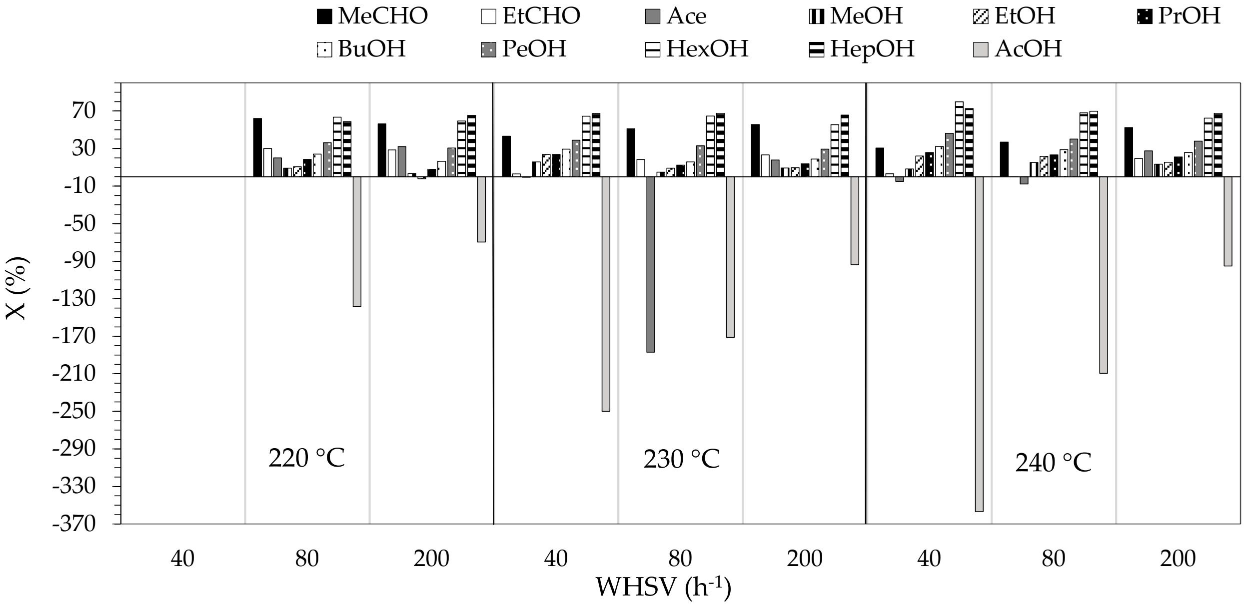

Figure S2. Individual conversion of ethanal (black), propanal (white), acetone (dark grey), methanol (vertical lines), ethanol (diagonal lines), propanol (black with white dots), butanol (white with black dots), pentanol (grey with white dots), hexanol (thin horizontal lines), heptanol (thick horizontal lines), and acetic acid (light grey) in APR at 4.5 MPa.

Appendix B. Equilibrium constants

The equilibrium constants of WGS and CO_2 methanation reactions were calculated with Eq. C.1 and using the parameters provided in Table S1, previously reported in [37]. The equilibrium constant of the WGS reaction was assumed the inverse of that for the reverse WGS (rWGS) reaction (Eq. C.2). The equilibrium constants for both reactions at the different temperatures applied for this study are presented in Table S2.

$$K_i = \exp\left[\frac{\lambda_1}{T^2} + \frac{\lambda_2}{T} + \lambda_3\right] \qquad (C.1)$$

$$K_{WGS} = {K_{rWGS}}^{-1} \qquad (C.2)$$

Table 1. Constants associated to calculation of temperature dependency of equilibrium coefficient [33]. .

	λ_1	λ_2	λ_3
rWGS	-191928.1	-3937.4	3.8143
CO_2 methanation	-730726	24125.3	-26.9616

Table S2. Equilibrium constant at different temperatures.

***T* (°C)**	210	220	230	240
K_{WGS}	174	143	118	98

$K_{CO2\ \mathrm{methanation}}$	419671699	172792699	73520934	32269518

Appendix C. Correlation matrixes

Table S3. Correlation matrix for model A.

	1	2	3	4	5	6	7	8	9
1	1								
2	0.967	1							
3	0.277	0.279	1						
4	-0.062	-0.114	0.053	1					
5	0.228	0.236	-0.001	-0.079	1				
6	-0.194	-0.02	0.012	-0.098	0.006	1			
7	-0.2	-0.365	0.04	0.194	-0.072	-0.627	1		
8	-0.105	-0.082	-0.027	-0.428	-0.06	0.161	-0.143	1	
9	0.977	0.998	0.297	-0.101	0.227	-0.047	-0.321	-0.088	1

Table S4. Correlation matrix for model B.

	1	2	3	4	5	6	7	8
1	1							
2	0.687	1						
3	-0.041	-0.062	1					
4	0.31	0.258	0.061	1				
5	0.062	0.074	-0.064	-0.023	1			
6	-0.585	0.087	0.018	-0.125	-0.01	1		
7	0.341	-0.132	0.123	0.134	0.025	-0.69	1	
8	-0.033	0.061	-0.015	-0.619	-0.023	0.138	-0.178	1
9	-0.752	-0.991	0.022	-0.286	-0.056	-0.008	0.033	-0.046

Table S5. Correlation matrix for model C.

	1	2	3	4	5	6	7	8
1	1							
2	-0.662	1						
3	-0.028	-0.245	1					
4	0.178	-0.242	0.062	1				
5	0.019	0.052	0.314	-0.027	1			
6	-0.872	0.578	0.013	-0.152	0	1		
7	0.544	-0.773	0.126	0.18	0.07	-0.671	1	
8	-0.122	0.153	-0.033	-0.643	-0.033	0.165	-0.213	1

Appendix D. Fit of model C

The fit obtained with model C for liquid and gas phase components at different space times for different temperatures and pressures is presented in Figure S3 - Figure S12.

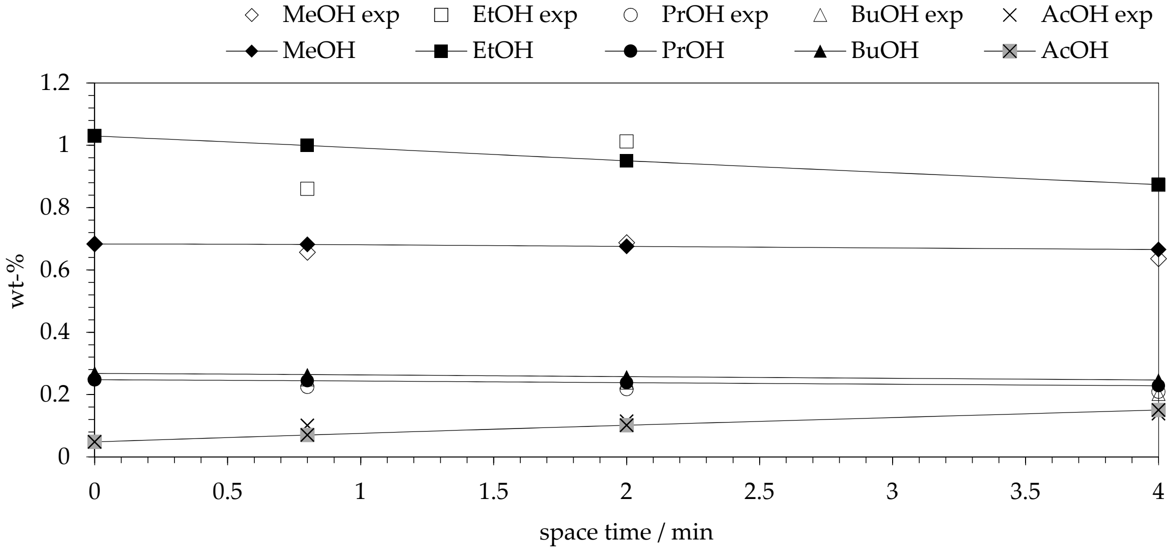

Figure S3. Experimental (empty symbols) and calculated (connected full symbols) weight concentrations of MeOH (diamond), EtOH (cube), PrOH (sphere), BuOH (triangle) and AcOH (cross) at 210 °C, 3.2 MPa and different reactor space-times.

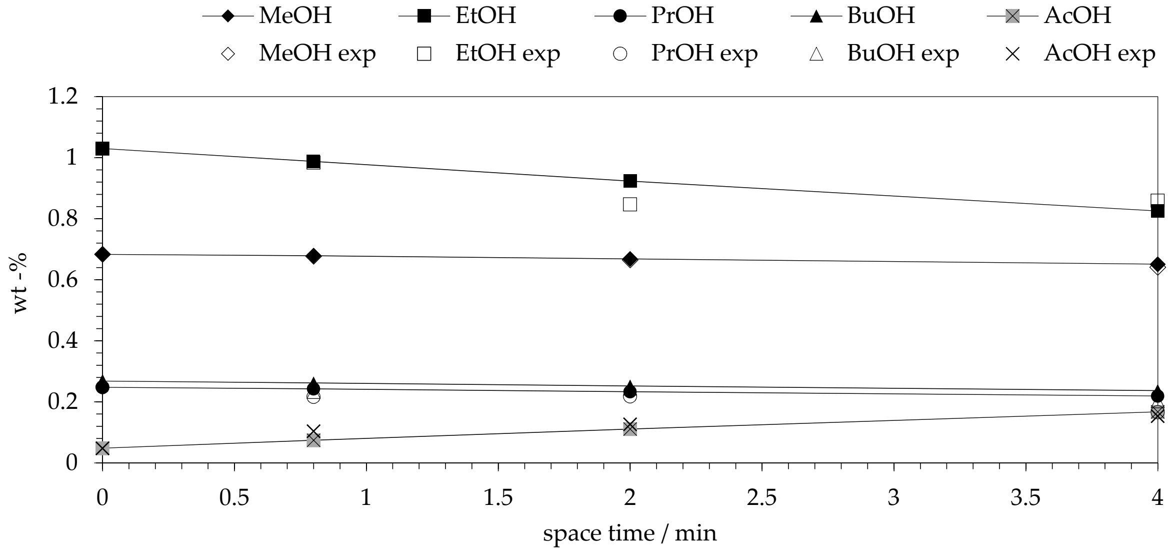

Figure S4. Experimental (empty symbols) and calculated (connected full symbols) weight concentrations of MeOH (diamond), EtOH (cube), PrOH (sphere), BuOH (triangle) and AcOH (cross) at 220 °C, 3.2 MPa and different reactor space-times.

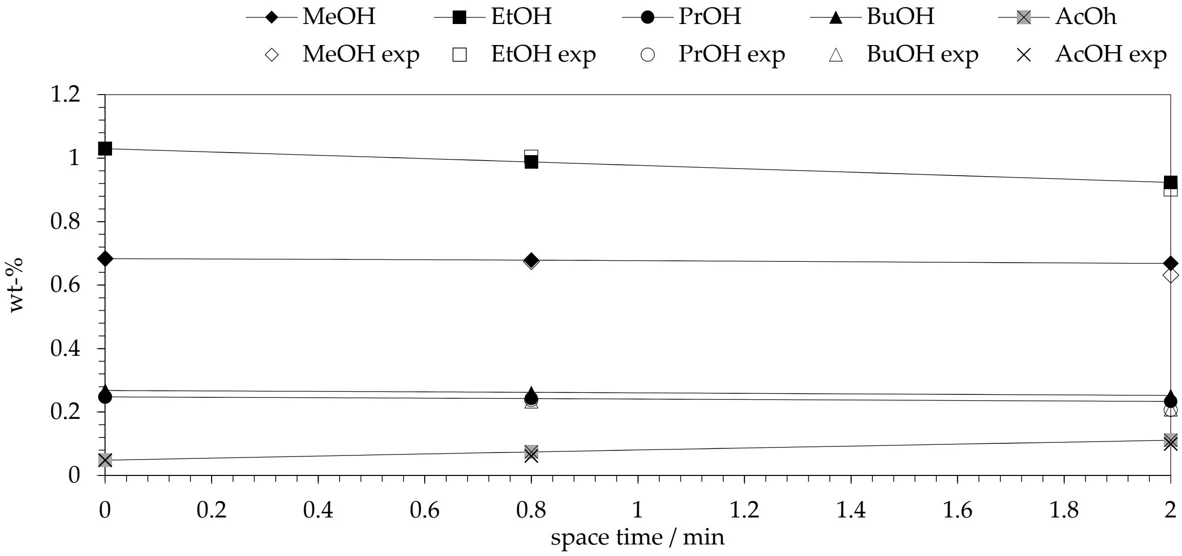

Figure S5. Experimental (empty symbols) and calculated (connected full symbols) weight concentrations of MeOH (diamond), EtOH (cube), PrOH (sphere), BuOH (triangle) and AcOH (cross) at 220 °C, 4.5 MPa and different reactor space-times.

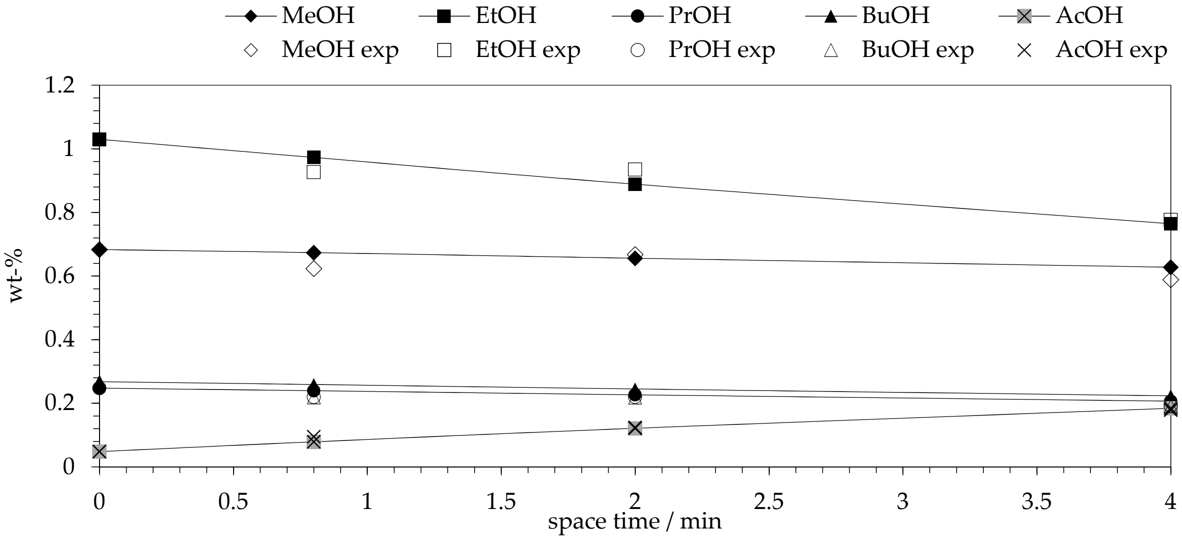

Figure S6. Experimental (empty symbols) and calculated (connected full symbols) weight concentrations of MeOH (diamond), EtOH (cube), PrOH (sphere), BuOH (triangle) and AcOH (cross) at 230 °C, 4.5 MPa and different reactor space-times.

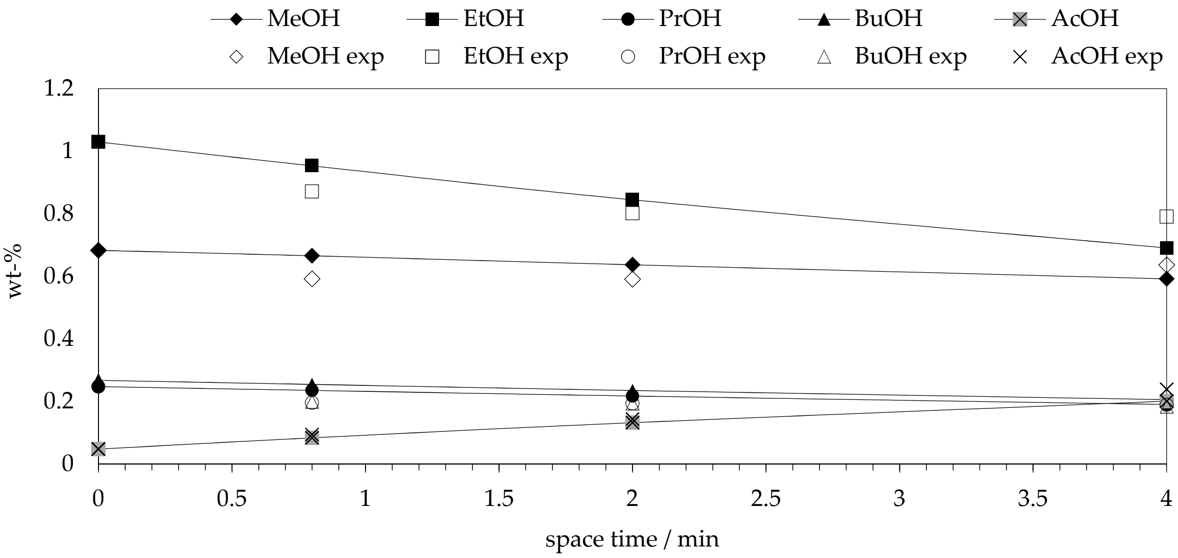

Figure S7. Experimental (empty symbols) and calculated (connected full symbols) weight concentrations of MeOH (diamond), EtOH (cube), PrOH (sphere), BuOH (triangle) and AcOH (cross) at 240 °C, 4.5 MPa and different reactor space-times.

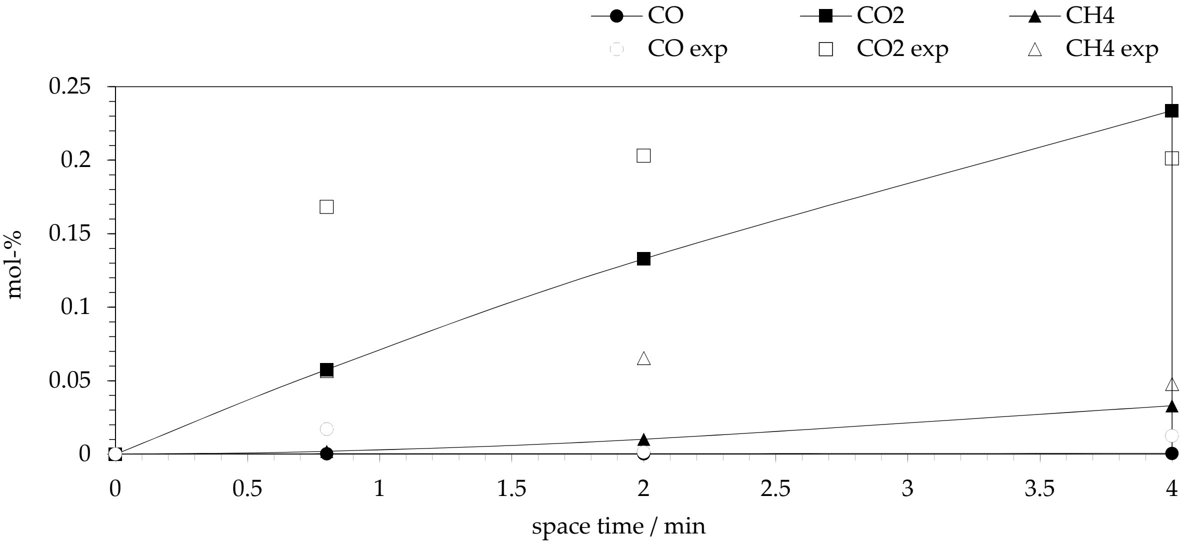

Figure S8. Experimental (empty symbols) and calculated (connected full symbols) molar concentrations of CO (sphere), CO_2 (cube) and CH_4 (triangle) at 210 °C, 3.2 MPa and different reactor space-times.

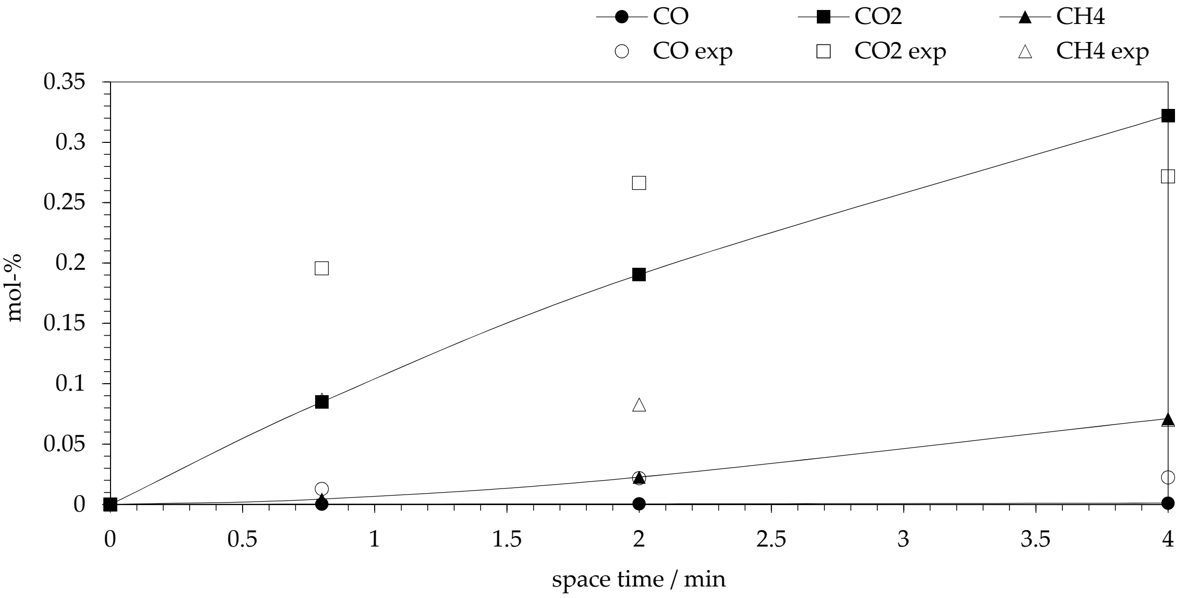

Figure S9. Experimental (empty symbols) and calculated (connected full symbols) molar concentrations of CO (sphere), CO_2 (cube) and CH_4 (triangle) at 220 °C, 3.2 MPa and different reactor space-times.

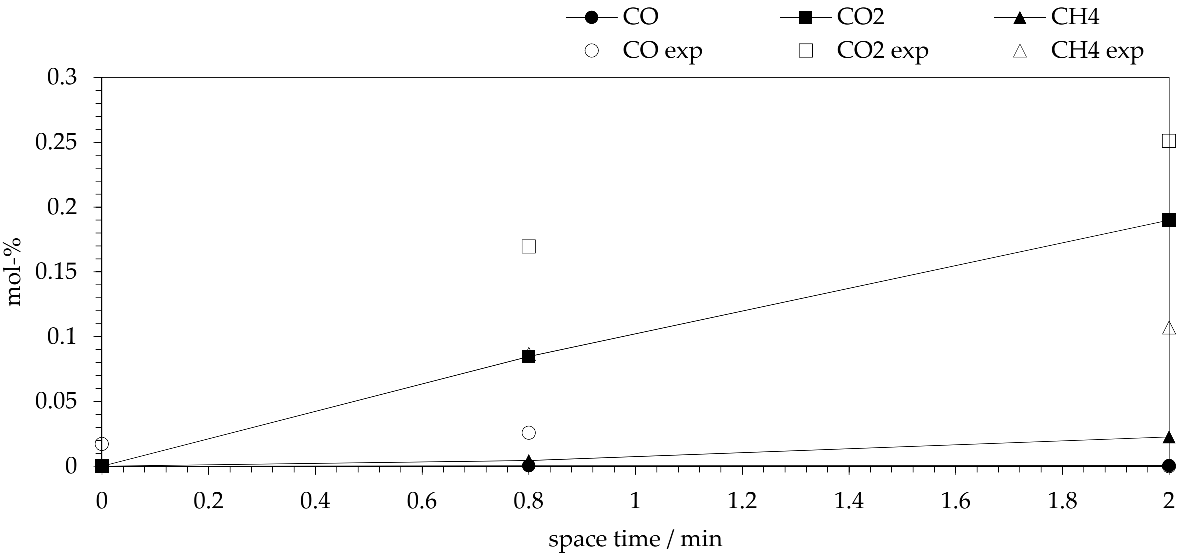

Figure S10. Experimental (empty symbols) and calculated (connected full symbols) molar concentrations of CO (sphere), CO_2 (cube) and CH_4 (triangle) at 220 °C, 4.5 MPa and different reactor space-times.

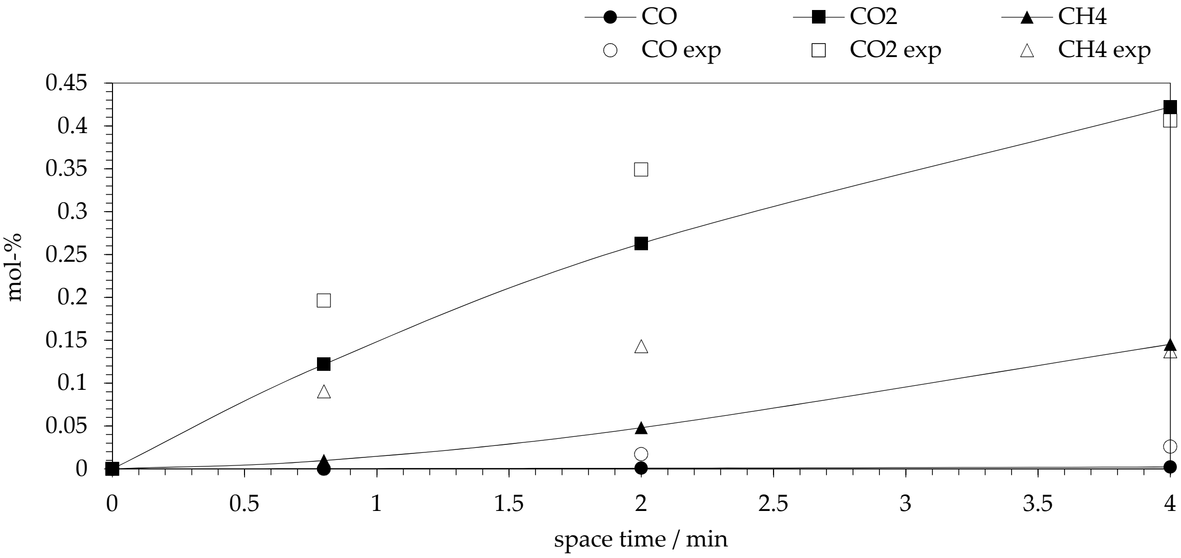

Figure S11. Experimental (empty symbols) and calculated (connected full symbols) molar concentrations of CO (sphere), CO_2 (cube) and CH_4 (triangle) at 230 °C, 4.5 MPa and different reactor space-times.

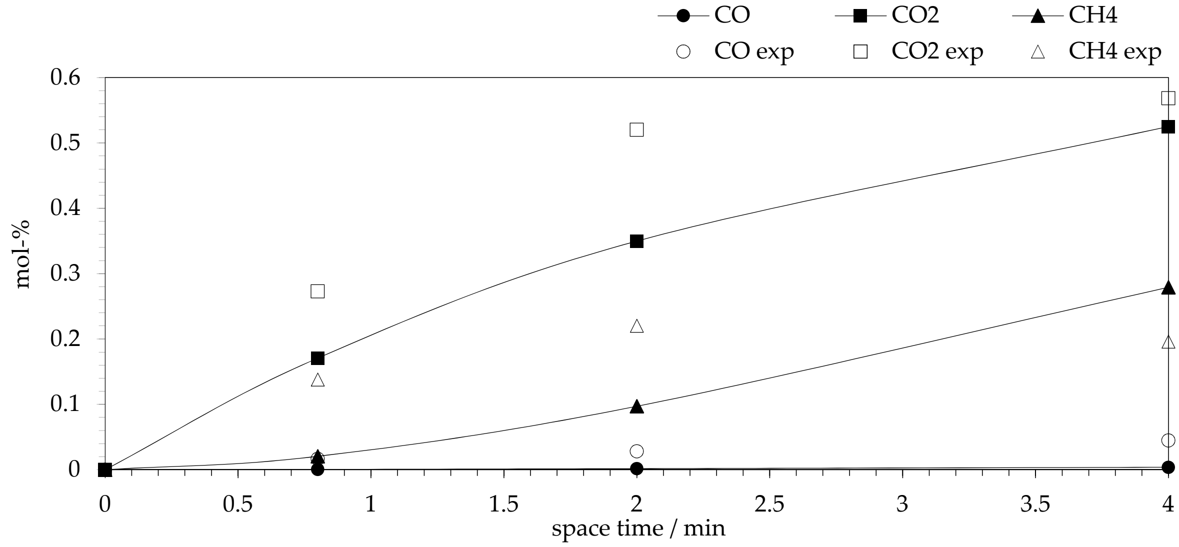

Figure S12. Experimental (empty symbols) and calculated (connected full symbols) molar concentrations of CO (sphere), CO_2 (cube) and CH_4 (triangle) at 240 °C, 4.5 MPa and different reactor space-times.

Appendix E. Catalyst characterization methods and results

E.1 Characterization methods

The metal loading of the calcined catalyst was analysed with atomic absorption spectroscopy (AAS). The sample analysed with AAS consisted of 200 mg of catalyst dissolved in aqua regia at 120 °C and diluted with Milli-Q water. The equipment used for the analysis of metal loading of both Ni and Cu was Varian AA240 (Santa Clara, CA, USA), and an air-acetylene flame was applied.

The support and the calcined catalyst were additionally characterized through nitrogen physisorption at -196 °C utilizing BET (Brunauer-Emmett-Teller) and BJH (Barrett-Joyner-Halenda) methods to determine the surface area, and the pore volume and average pore diameter. The equipment utilized was a Micromeritics 3 Flex (Norcross, GA, USA) where a sample of 0.77 g of catalyst was analysed after degassing at 180 °C for 17 h in vacuum.

The X-ray diffraction (XRD) data for the support and the calcined catalyst were obtained in a PANalytical X-pert PRO MPD Alpha-1 diffractometer (Malvern, WR14, United Kingdom) with Cu Kα1 radiation (45 kV and 40 mA). The continuous scanning ranged from 10° to 90° (2θ) with step size of 0.0131°.

E.2 Characterization results

The metal content of the calcined catalyst and the surface properties of the support and the calcined catalyst are presented in Table S6. Nickel and copper contents, 9.5 and 4.5 wt-% respectively, were close to the targeted amounts, which confirms a successful impregnation.

After the impregnation of metals and calcination of the catalyst, the support micropores might have been partially blocked, which resulted in a decrease in the surface area, pore volume and average pore diameter.

Table 6. Catalyst metal content and textural properties determined with AAS and N_2 physisorption respectively.

			AAS	N_2 physisorption		
		Ni/Cu target (mass fraction)	Ni/Cu (mass fraction)	BET surface area ($m^2 \cdot g^{-1}$)	Pore Volume ($cm^3 \cdot g^{-1}$)	Average pore diameter (nm)
25CeZr	Support	n.a.	n.a.	99[a]	0.28[a]	10.7[a]
NiCu/25CeZr	Calcined	10 % / 5 %	9.5 % / 4.5 %	72	0.20	8.3

n.a.: not applicable.

[a] Reported in [13].

The diffractograms included in Figure S13 show the characteristic peaks of NiO at 2θ positions 37° and 44°, and CuO at 38° 2θ for the calcined catalyst (NiCu/25CeZr) compared to the support, prior metal impregnation (25CeZr).

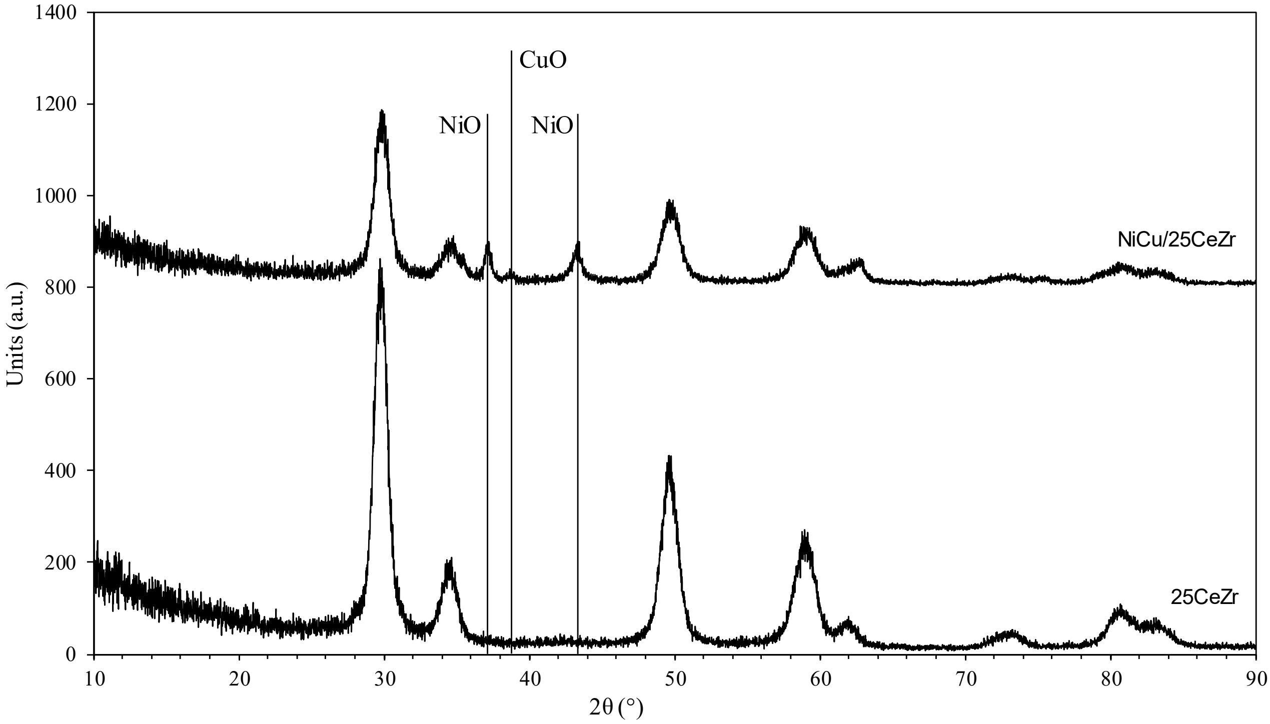

Figure 13. X-ray diffractograms of 25CeZr and calcined NiCu/25CeZr. NiO and CuO peaks are indicated with vertical lines.